Detailed comparison of glaciological and geodetic mass balances for Urumqi Glacier No.1, eastern Tien Shan, China, from 1981 to 2015

Chunhai Xu[a,b,*], Zhongqin Li[a,**], Puyu Wang[a], Muhammad Naveed Anjum[a,b], Huilin Li[a,b], Feiteng Wang[a]

[a] State Key Laboratory of Cryospheric Science/Tien Shan Glaciological Station, Northwest Institute of Eco-Environment and Resources, Chinese Academy of Sciences, Lanzhou 730000, China
[b] University of Chinese Academy of Sciences, Beijing 100049, China

ABSTRACT

The mass balance of Urumqi Glacier No.1, eastern Tien Shan, has been monitored since 1959, using the direct glaciological method. This study presents a detailed comparison of the glaciological mass balance with a high-quality product of geodetic surveys in the overlapping period from 1981 to 2015. We analyzed the generic differences between glaciological and geodetic mass-balance measurements, including in-depth uncertainties assessments. The statistical comparison shows that the reduced discrepancy ($\delta = 0.53$) between the geodetic mass balance (-0.53 ± 0.14 m w.e. a^{-1}) and corrected annul glaciological mass balances (-0.46 ± 0.14 m w.e. a^{-1}) falls within the 95% confidence interval and reveals that no statistical significant bias between the two datasets is detectable over the period. Thanks to the good agreement, calibration of the glaciological to the geodetic data series is currently not required. The more negative geodetic mass balance is probably relevant to the glacier surface characteristics. The uncertainty of our results measured with geodetic method was close to the majority of similar studies, but bigger than those derived from multi-temporal high-quality DEMs. Further studies should continue using a long-range terrestrial laser scanning (TLS) system to derive high-resolution and -precision digital elevation models (DEMs) of the glacier surface at the monthly time-scale, which will provide a powerful complement to the glaciological measurements.

1. Introduction

Populations in Central Asia depend largely on glacier melt for their water supplies and this situation is well reflected in the Tien Shan (Farinotti et al., 2015). Glacier mass balance provides direct information on the gain or loss in glacier ice, which are crucial for studying the impact of mass changes to water resources, sea level rise and climate-glacier interactions (Kaser et al., 2006; Zemp et al., 2015). Mass balance is commonly obtained by the direct glaciological method, which provides in situ measurements of annual and sometimes seasonal mass balance using stakes and snow pits at the end of the hydrological year (Østrem and Brugman, 1991; Xie and Liu, 1991; Zemp et al., 2013). Mass balance can also be assessed indirectly using the geodetic method, in which two digital elevation models (DEMs) of the glacier surface are subtracted to calculate the volume changes, which is then converted to mass using a density conversion (Cogley et al., 2011). The glaciological method measures the surface mass balance, which can provide better understanding of glacier melt, and the geodetic measurements include surface, internal and basal mass balances. Comparison of glaciological and geodetic measurements has been widely studied (Cogley, 2009; Thibert and Vincent, 2009; Fischer, 2011). Some studies have shown good agreement, such as Storglaciären, Sweden (Zemp et al., 2010) and White Glacier, Canada (Thomson et al., 2017). Some studies showed significant discrepancy: for example Hagg et al. (2004) compared the two methods calculating mass balance of the Tuyuksu Glacier (Kazakhstan) and the difference was -4.2 m w.e. over 40 years. This discrepancy can be explained mainly by deficiencies in the glaciological measurements. For Abramov glacier (Kyrgyzstan), the disagreement was -0.48 m w.e. a^{-1} from 2000 to 2011, which can be explained by an underestimation of the SRTM C-band penetration depth into snow (Barandun et al., 2015). In some cases, the glaciological method implies systematic errors in one direction which increase linearly with the

number of seasonal and annual measurements (Cox and March 2004; Thibert et al., 2008; Huss et al., 2009). Zemp et al. (2013) proposed a framework for assessment of random and systematic errors, as well as for validation and calibration of the glaciological series with the geodetic balance results.

Within the international glacier monitoring strategy, the strength of the geodetic method is that it provides decadal to sub-decadal values that take into account the entire glacier, including inaccessible areas. Its results are essential for validating and calibrating the glaciological data series (Zemp et al., 2015). The validation and calibration is predicated on the geodetic balance being accurate, which primarily depends on the quality of DEMs used to derived glacier volume changes. The available DEMs are usually of limited spatiotemporal resolution, which is the main constraint for the computation of reliable geodetic mass balance. Airborne and terrestrial Light Detection and Ranging (LiDAR) techniques have offered dense point clouds and high-resolution and -precision DEMs of glacier surface terrain (Joerg et al., 2012; Helfricht et al., 2014; Piermattei et al., 2015; Fischer et al., 2016). Terrestrial laser scanning (TLS) often has error margins in the range of a few centimeters (Hartzell et al., 2015). Fischer (2011) concluded that the accuracy of geodetic mass balance in Apline regions resulting from the accuracy of the DEMs ranges from 1 m w.e. a^{-1} for photogrammetric data to 0.001 m w.e. a^{-1} for LiDAR data. Gabbud et al. (2015) applied a new generation of TLS which can be used to investigate a glacier surface ablation at the seasonal and hourly scales. Fischer et al. (2016) showed that repeated TLS surveys yielded accurate results for annual geodetic mass balances of very small glaciers in the Swiss Alps. Compared to airborne laser scanning (ALS), the terrestrial laser scanning technique is an easier and more cost-effective way of monitoring the individual glacier mass balance (Gabbud et al., 2015; Fischer et al., 2016; Xu et al., 2017).

To date, direct glaciological measurements are available for a few hundred glaciers and there are currently 41 reference glaciers with > 30 years of data in the World Glacier Monitoring Service (WGMS) time series (WGMS, 2017); geodetic surveys are currently available for 450 glaciers (Zemp et al., 2015). Urumqi Glacier No.1 located in the eastern Tien Shan, with the longest and most detailed surface mass balance measurement time series in China. The long-term mass balances were observed beginning in 1959 (Li et al., 2011). Its surface topography has been surveyed nine times at intervals of several years from 1962 to 2012 (Chen et al., 1996; Wang and Shen, 2011; Wang et al., 2016). A long-range Riegl VZ®-6000 terrestrial laser scanner was utilized to survey the glacier surface in 2015 and subsequently a high-resolution and accurate DEM was generated. Urumqi Glacier No.1 can be considered as a well-suited test site to compare the glaciological and geodetic measurements.

Urumqi Glacier No.1 was taken here as a case study to compare the obtained results between the glaciological and the geodetic methods over the period of record (PoR, 1981–2015). The following research questions for this study were defined: What is the source of the observed uncertainties in both methods? To what extent the obtained results influenced by the different DEMs used, the existing snow cover, the reference area and processes of internal accumulation and ablation?

2. Study site

Urumqi Glacier No.1 (43°06′N, 86°49′E) is a northeast-orientated small valley glacier at the headwaters of the Urumqi River with an area of 1.59 km² and a length of 1.99 km in 2012 (Wang et al., 2016), situated on the northern slope of Tianger Summit II (4848 m a.s.l.) in the eastern Tien Shan (Fig. 1). The area of Urumqi Glacier No.1 decreased strongly over the PoR. The glacier area was 1.56 km² on 2 September 2015 based on TLS-derived high-resolution DEM. Compared with the glacier extent derived from the map in 1981, the overall area loss was 0.30 km² (−16.4%), the shrinkage rate is higher than the investigated glaciers in the Chinese Tien Shan (−11.5%) (Wang et al., 2011).

Note that Urumqi Glacier No.1 is a summer-accumulation-type glacier in a continental climate setting. Both accumulation and ablation occur simultaneously during summer (Li et al., 2011). The two branches (east and west branches) of the glacier separated completely in 1993 due to continued glacier retreat (Li et al., 2010). The glacier was for the first time monitored in 1959, and mass-balance data have been recorded in Annual Reports of the Tien Shan Glaciological Station from 1980 to present and published in the Glacier Mass Balance Bulletin (every two years) compiled by the WGMS (http://wgms.ch/). Urumqi Glacier No.1 is also one of the reference glaciers in the WGMS glacier monitoring network and a representative glacier in Central Asia (Zemp et al., 2009; Li et al., 2011).

3. Data and methods

3.1. Riegl VZ®-6000 TLS

Common TLS systems use class 1 laser beams with wavelengths around 1500 nm, with low reflectance over snow and ice cover, and the possible scanning distance is restricted to a few hundred meters, limiting the application of TLS surveys for glacier studies (Rabatel et al., 2008; Deems et al., 2013; Fischer et al., 2016). A new generation of Riegl VZ®-6000 TLS typically uses class 3B laser beams (wavelengths around 1064 nm); the instrument is, due to its laser wavelength, exceptionally well suited for measuring snowy and icy terrain in glacier mapping (Fischer et al., 2016). Faster surveys (up to 222,000 measurements s^{-1}) are possible, even at long range (better than 6000 m), with unprecedentedly high accuracy and precision (RIEGL Laser Measurement Systems, 2014a).

Based on time-of-flight measurement with echo digitization and online waveform processing, the Riegl VZ®-6000 TLS can capture repeated dense point clouds of the glacier surface terrain with emitting near-infrared laser signals (RIEGL Laser Measurement Systems, 2013). The laser pulse transmitter emits a laser pulse, which is reflected by the target object back to the laser receiver, and used to calculate the distance between object and sensor (RIEGL Laser Measurement Systems, 2014a).

3.2. TLS field surveying

On 2 September 2015 (at the end of the mass balance year), Riegl VZ®-6000 surveys of Urumqi Glacier No.1 were performed for four scan positions (Fig. 2), on the same day as the glaciological measurements. Each scan position was fixed on the stable bedrock using a reinforced concrete structure with a GPS-leveling point at the terminus of the glacier, and the instrument was mounted on a tripod for each scan position to prevent ground motion and guarantee data quality. Three-dimensional (3-D) coordinates of the four scan positions were obtained using the real-time kinematic (RTK) global positioning system. The accuracy of this type of RTK surveys has been reported to be within ± 1 cm horizontally and ± 2 cm vertically, according to previous studies on Urumqi Glacier No.1 (Wang et al., 2016; Xu et al., 2017). The coordinate system of RTK surveys is the World Geodetic System 1984 (WGS84).

The surveying parameters were configured as a compromise between ensuring high-level data quality and minimizing acquisition time. In order to avoid range ambiguity and to obtain the maximum scanning range of the glacier surface, coarse scanning was first implemented with vertical and horizontal angles range of 60–120° from zenith and 0–360°, respectively, and the laser pulse repetition rate was set to 50 kHz. On the basis of coarse scanning, we selected glacier surface terrain regions, and laser pulse repetition rate was then set to 30 kHz to carry out fine scanning for the regions of interest. The overlap percentage of each scan was not < 30% to meet the requirements of multi-station adjustment (MSA) (Mukupa et al., 2016). Surveying parameters of Urumqi Glacier No.1 are given in Table 1.
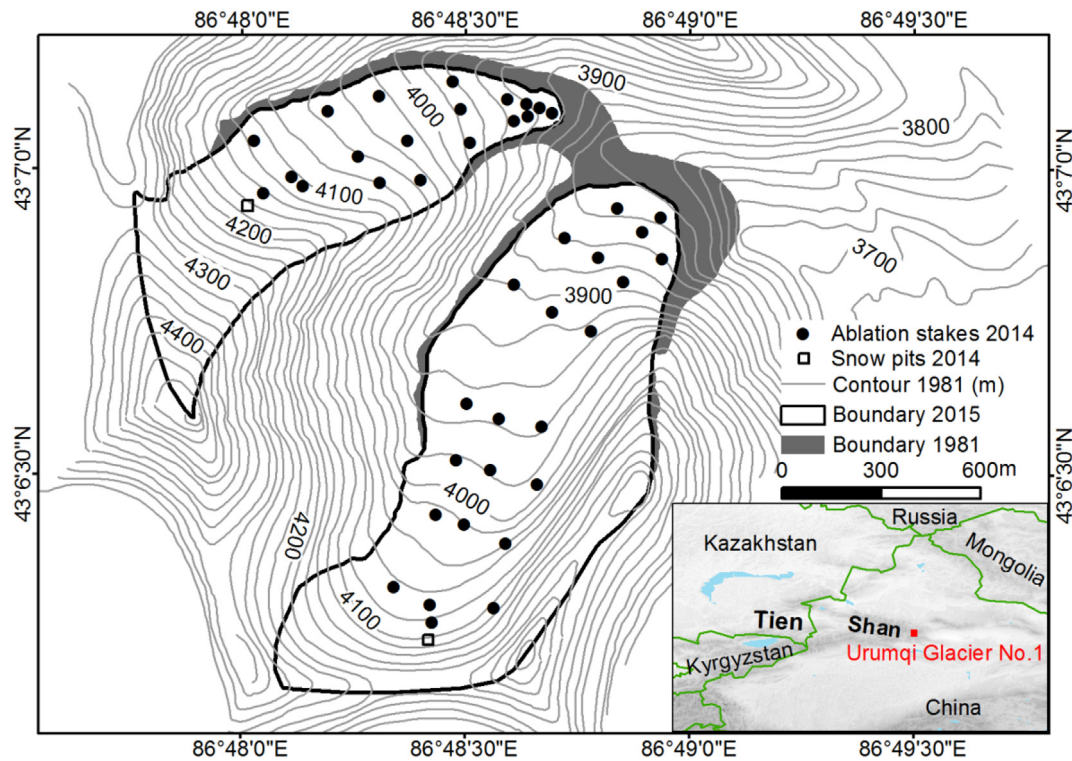
Fig. 1. Study site. Location map of Urumqi Glacier No.1, eastern Tien Shan, and measuring network in 2014 for glaciological mass balance. Contour and boundary 1981 derived from the topographic map. Boundary 2015 was delineated from a TLS-derived high-resolution DEM.

3.3. Point cloud processing

RiSCAN PRO® v1.81 software was used to perform the point cloud data processing (RIEGL Laser Measurement Systems, 2014b). This included three steps:

I. Direct georeferencing. We used additional sensors (e.g. navigation sensors, total station, etc.) to georeference the laser scanner's system (Mukupa et al., 2016). RTK surveying points of each scan position were used to transform the Scanner's Own Coordinate System (SOCS) into a Global Coordinate System (GLCS). The fundamentals are given by the vector equation (Lichti et al., 2005):

$$\vec{r_g} = \vec{r_0} + R(k)\vec{r_s} \tag{1}$$

where $\vec{r_g}$ is the vector of the target in the GLCS; $\vec{r_s}$ is the vector of the same target in the SOCS; $\vec{r_0}$ is the vector of SOCS origin in the GLCS; k is the derived azimuth from the scan position to the backsight station and

$$R(k) = \begin{Bmatrix} \cos k & \sin k & 0 \\ \sin k & \cos k & 0 \\ 0 & 0 & 1 \end{Bmatrix} \tag{2}$$

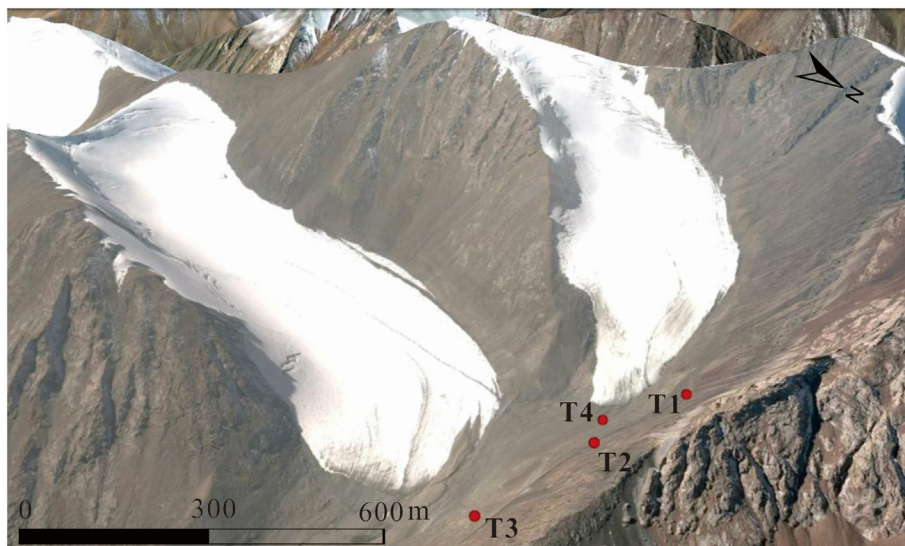II. Point cloud registration. After direct georeferencing, the position of

Fig. 2. Spatial distribution of four TLS scan positions at the glacier terminus, each scan position was fixed using reinforced concrete with a GPS-leveling point. Scan position T1 and T4 captured the surface point clouds of the west branch and T2 and T3 those of the east branch (image source: Google Earth).

Table 1
Riegl VZ®-6000 TLS surveying parameters of Urumqi Glacier No.1 on 2 September 2015.

Scan positions	Scanning range m²	Number of points	Point density m⁻²	Angle increment* °	Scanning time min
T1	1 532 007.89	7 560 104	4.93	0.046	22
T2	1 845 433.80	21 768 108	11.80	0.020	30
T3	951 051.05	19 581 210	20.59	0.019	26
T4	844 129.58	16 591 327	19.65	0.019	25

* The vertical and horizontal angle increment were configured the same.

each scan was fixed, whereas, because of the influence of orientation, the point clouds of the overlapped regions cannot coincide completely (Fig. 3a). The iterative closest point (ICP) algorithm was used to realize multi-station adjustment (Besl and McKay, 1992; Zhang, 1992). The orientation of each scan was iteratively modified to calculate the best fit between the points patches based on least-squares minimization of residuals until point cloud layers of each scan coincided (Fig. 3b) (Besl and McKay, 1992).

III. Point cloud vacuation and filtering. We used an octree algorithm to realize point cloud data reduction (vacuation), i.e. the algorithm was applied to the registered scans to generate points with equal spacing (Schnabel and Klein, 2006; Perroy et al., 2010). A terrain filter was then used to remove noise and non-ground points (RIEGL Laser Measurement Systems, 2014b). Then visual interpretation was performed to check the data and remove clear visual outliners. Finally, the overlapped point clouds of the four scan positions were merged into one layer.

Using ArcGIS10.1 software, a TLS-derived DEM was generated with a spatial resolution of 1 m. The DEM was then down-scaled to 30 m resolution to coincide with the topographic map (Section 3.4).

3.4. Co-registration of DEMs and topographic map

This study uses a 1:50,000-scale topographic map, which was derived from aerial photography in September 1981, established in July 1984 and published in 1986. The coordinate system of the map is Beijing 1954 and the elevation system used is Yellow Sea system 1956. The map was scanned at a resolution of 600 dpi to guarantee high precision. Using ENVI 5.1 software, the map was registered into Beijing 1954 coordinate system based on a kilometer grid and then converted into WGS84.

The TLS-derived DEM and the topographic map were misaligned in space as they were produced using different surveying techniques. Thus, a co-registration of the two DEMs was necessary before extracting glacier elevation changes (Nuth and Kääb, 2011). Considering the high resolution of the TLS-derived DEM, several clearly distinguishable

features over stable terrain were extracted as reference to register the topographic map. The 20 m contour lines of the 1981 map were digitized manually (Fig. 1), and a DEM was generated with a resampling spatial resolution of 30 m afterwards (Shangguan et al. 2010; Wei et al. 2015). According to the photogrammetric Chinese National Standard, the nominal vertical accuracy of the topographic map was better than 5 m for flat areas with slopes < 6° and 8 m for mountainous areas with slopes of 6–25° (GB/T 12343.1-2008, 2008). The calculated mean slope of Urumqi Glacier No.1 was about 21° in 1981. The vertical accuracy of the map is estimated to be better than 8 m on the glacierized terrain. As the topographic map provides fine depictions of glacier surface terrain, it has been used for geodetic mass balance calculations (Andreassen, 1999; Paul and Haeberli, 2008).

3.5. The glaciological method

3.5.1. Glaciological measurements

The glaciological mass balance of Urumqi Glacier No.1 has been observed since 1959 by measuring stakes and snow pits (Han et al., 2005; Xie and Liu, 2010). The glaciological measurements were interrupted during the period 1967–1979 (Han et al., 2005), and the glaciological mass balance data series during this period were estimated from correlations with climatic data observed at the Daxigou Meteorological Station (3539 m a.s.l.), situated about 3 km southeast of Urumqi Glacier No.1 (Li, 2005; Li et al., 2011). The program was restarted in 1980 using ablation stakes and snow pits. Not < 40 ablation stakes were drilled into the glacier surface evenly distributed at different elevation bands of the east and west branch using a stream drill (Figs. 1, 4 and 5c). Usually, from the beginning of May to early September each year, a spatial distribution of single-point ablation and accumulation were determined by stakes and snow pits at monthly intervals. The net accumulation is measured by digging snow pits at each of the stakes in the area of the glacier where snow has accumulated during the period of investigation; stakes are drilled into the glacier and change in an exposed stake height plus change in snow depth (if snow exists) at two successive dates gives the net ice ablation at this point (Kaser et al., 2003; Xie and Liu, 2010). Thus the measured items of Urumqi Glacier No.1 include stake vertical height over the glacier surface, thickness of superimposed ice, and thickness and density of each snow/firn layer at individual stakes.

3.5.2. Determination of glaciological mass balance

Glaciological mass balance includes point and glacier-wide mass balances, and the point mass balance Δm over the span time from t_0 to t_1 is related to the mass-balance rate $\dot{m}$ (Cogley et al., 2011):

$$\Delta m = \int_{T_0}^{T_1} \dot{m}(t)dt = m(t_1) - m(t_0) \tag{3}$$

point values can be extrapolated to glacier-wide mass balance using the contour-line or profile method (Østrem and Brugman, 1991; Kaser et al., 2003). For Urumqi Glacier No.1, contour-line and isoline methods had been successfully used to calculate glacier mass balance (Fig. 4) (Xie and Liu, 1991). The glaciological mass-balance data series
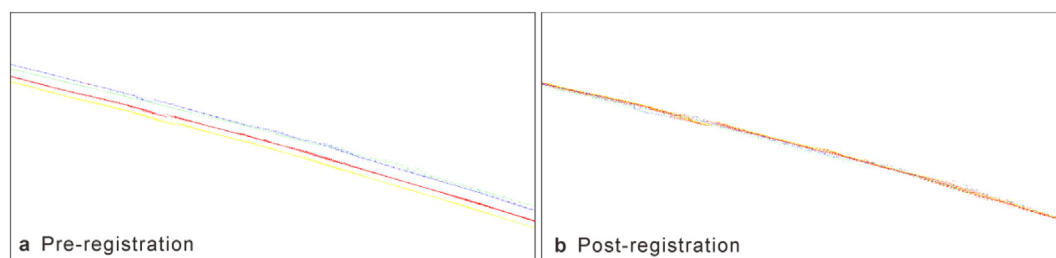

Fig. 3. Comparison between pre- and post-registration point cloud layers in profile. Blue, yellow, red and green indicate the point cloud layer of scan position T1, T2, T3 and T4, respectively. (For interpretation of the references to colour in this figure legend, the reader is referred to the web version of this article.)
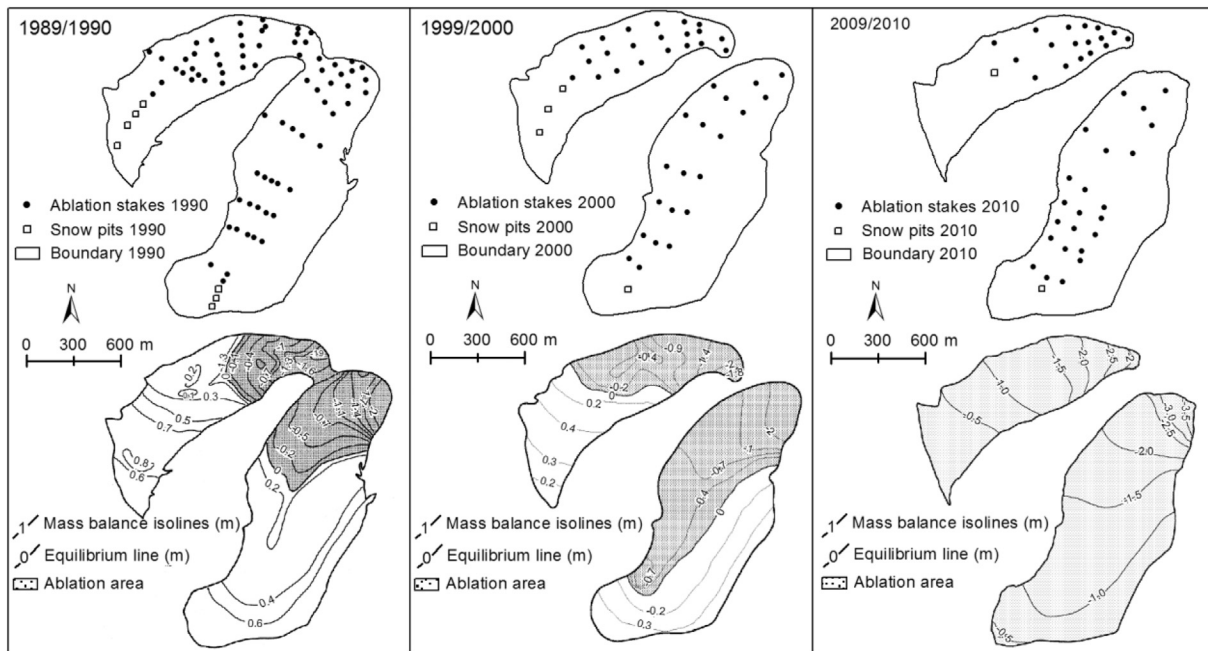
Fig. 4. The locations of the glaciological mass balance measurements (top) and mass balance isoline map (bottom) for three mass-balance years 1989/1990, 1999/2000 and 2009/2010. Shading marks positive mass balance and white marks negative mass balance.

used in this paper were originated from WGMS and the Annual Report of the Tien Shan Glaciological Station.

3.6. The geodetic method

The geodetic mass balance of Urumqi Glacier No.1 over the PoR was calculated based on the subtraction of two high-resolution DEMs. The total volume change $\triangle V$ was determined by summing the elevation change $\triangle h_i$ at the individual pixel r of different time periods:

$$\triangle V = r^2 \sum_{i=1}^{N} \triangle h_i \tag{4}$$

where N is the number of pixels covering the glacier at the maximum extent, and r is the pixel size (30 m × 30 m).

The calculated volume change must be converted to geodetic mass balance (m w.e.) following:

$$B_{\text{geod}} = \frac{\triangle V}{\overline{S}} \cdot \frac{\rho}{\rho_{\text{water}}} = \frac{\triangle V}{\frac{S_{t2} + S_{t3}}{2}} \cdot \frac{\rho}{\rho_{\text{water}}} \tag{5}$$

where ρ is the average density of $850 \pm 60 \, \text{kg m}^{-3}$ as described in Section 5.1 and $\overline{S}$ is the mean glacier area over the PoR, the two acquisition dates $t2$ and $t3$, assuming a linear change (Thibert et al., 2008; Zemp et al., 2013).
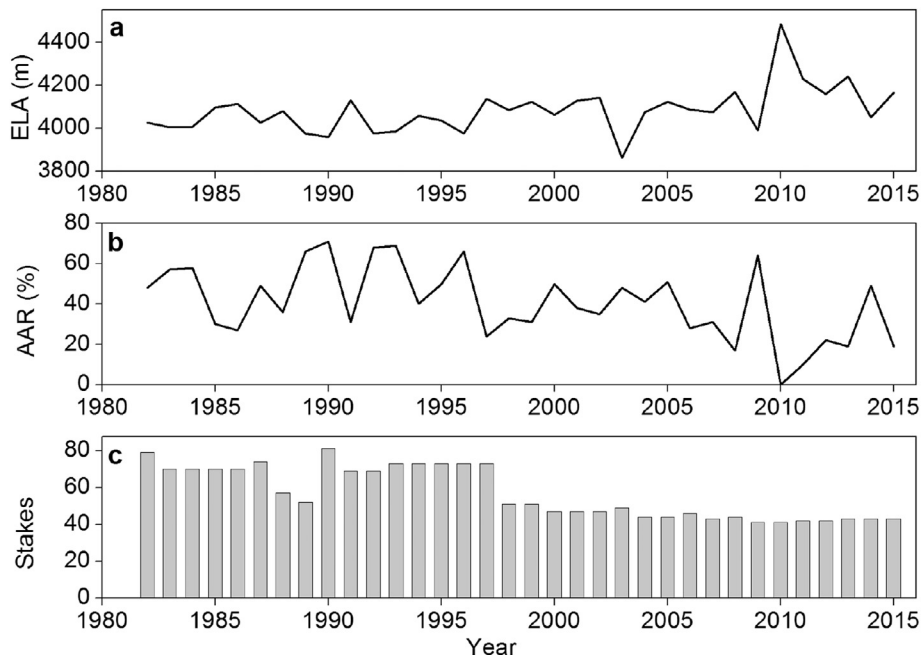

Fig. 5. (a) The equilibrium-line altitude (ELA) of Urumqi Glacier No.1 over the PoR; (b) accumulation-area ratio (AAR); and (c) number of ablation stakes in the glaciological measuring network.
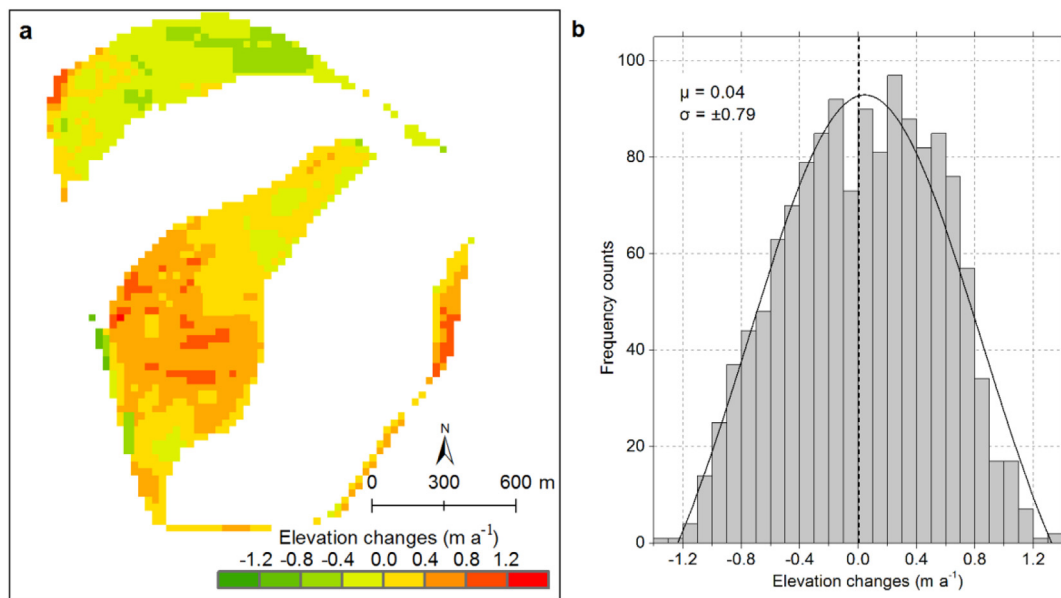
Fig. 6. (a) Spatial distribution of mean annual surface elevation changes over stable terrain by differencing of the two DEMs. (b) Frequency distribution of stable terrain elevation differences and the black curve is normal fit (gaussian distribution) over the frequency counts. The mean (μ) and standard deviation (σ) of the elevation changes are listed.

4. Uncertainty assessment

4.1. Uncertainties of glaciological measurements

Uncertainties related to the glaciological mass balance are not easy to evaluate due to the main source of errors is not properly understood. The source and magnitude of errors may be affected by climate conditions, glacier surface topography, glacier size and inaccessible glacier areas (e.g. crevasses, steep ice and debris cover, etc.) for in situ measurements (Dyurgerov, 2002). Meier et al. (1971) indicated that glaciological measurement errors range from ± 0.1 to ± 0.34 m w.e. for glacier-wide annual mass balance. Related studies estimated an error of ± 0.2 m w.e in the calculation of point and glacier-wide mass balance using the glaciological method (Dyurgerov, 2002). Uncertainties of glaciological measurements were categorized as follows:

1. Field observations. Point measurement uncertainties are related to errors in stake readings and snow/firn probing (Jansson and Pettersson, 2007; Huss et al., 2009), the sinking of the stakes or the false determination of the firn layer surface at the end of the last hydrological year (Zemp et al., 2010). For uncertainty in point annual mass balance: some studies have calculated an error of ± 0.14 m w.e. for ablation measured in ice, ± 0.27 m w.e for ablation measured in firn and ± 0.21 m w.e. for accumulation (Thibert et al., 2008); others have quantified errors of ± 0.1 and ± 0.3 m w.e. for reading stakes in the ablation and accumulation areas, respectively (Huss et al., 2009).

2. Extrapolating point measurements to the whole glacier. The error source mainly includes extrapolating observed values to unmeasured areas, insufficient spatial distribution of measured sites and the interpolation method (Fischer et al., 2016). Hock and Jensen (1999) estimated the error of the interpolation method to about ± 0.1 m w.e. a^{-1} for mean specific mass balances. Huss et al. (2009) computed and compared mean specific net balance with randomly reduced annual stake datasets and found an error of ± 0.12 m w.e a^{-1}.

3. Using non-updated glacier area to calculate glacier mass balance (Elsberg et al., 2001; Huss et al., 2012). Glacier retreat results in an overestimate of glacier mass loss. For Urumqi Glacier No.1, the maximum, minimum and average errors in the reduction area amounted to 4.5%, 2% and 3.5% of glacier-wide annual mass balance, respectively, from 1988/1989 to 2005/2006 (Wang and Shen, 2011). Here we used this error term as the stochastic uncertainty related to the reference

glacier area.

By taking into account the above-mentioned factors, the annual uncertainty in glacier-wide mass balance ($\sigma_{\text{glac. a}}$) can be calculated as

$$\sigma_{\text{glac.a}} = \sqrt{\sigma_{\text{field}}^2 + \sigma_{\text{extra}}^2 + \sigma_{\text{area}}^2} \tag{6}$$

where σ_{field}, σ_{extra} and σ_{area} are errors related to field measurements, extrapolation of point values to glacier-wide mass balance and the non-updated area, respectively (Huss et al., 2009; Zemp et al., 2010). Here we take $\sigma_{\text{field}} = \pm 0.1$ m w.e. a^{-1}, $\sigma_{\text{extra}} = \pm 0.1$ m w.e. a^{-1} and $\sigma_{\text{area}} = \pm 0.02$ m w.e. a^{-1}, conservatively. The annual uncertainty of glaciological mass balance was ± 0.14 m w.e. a^{-1}, and cumulative uncertainty ($\sigma_{\text{glac. PoR}}$) was calculated to be ± 0.83 m w.e over the PoR (N years).

$$\sigma_{\text{glac.PoR}} = \sigma_{\text{glac.a}} \cdot \sqrt{N} \tag{7}$$

4.2. Uncertainties of geodetic mass balance

Uncertainties in the geodetic mass balance are mainly related to the accuracy of the DEMs used, and the density used to convert volume to mass change. The accuracy of the topographic map and TLS-derived DEM has been discussed in Sections 3.2 and 3.4. Here $\sigma_\rho = \pm 60$ kg m^{-3} is assumed as the uncertainty in density of volume change (Huss, 2013). The mean annual uncertainties of the geodetic mass balance ($\sigma_{\text{geod. a}}$) over the PoR can be estimated using (Huss et al., 2009)

$$\sigma_{\text{geod.a}} = \sqrt{\overline{\Delta h}^2 \sigma_\rho^2 + \rho^2 \sigma_{\Delta h}^2} \tag{8}$$

where $\overline{\Delta h}$ is the glacier-wide mean of geodetic elevation changes and $\sigma_{\Delta h}$ is the uncertainty relying on the accuracy of the two DEMs. There are no better ways to evaluate the uncertainty of DEMs without precise and well-distributed stable points (Bolch et al., 2017). The standard deviation of the non-glacierized stable terrain can be considered as a criterion for evaluating the uncertainty $\sigma_{\Delta h}$ (Gardelle et al., 2013; Fischer et al., 2016) and can be approximated using

$$\sigma_{\Delta h}^2 = \frac{\sigma_{\Delta hi}^2}{N_{\text{eff}}} \tag{9}$$

where $\sigma_{\Delta hi}$ is the standard deviation of the mean annual elevation change Δh in each elevation band (Fig. 6). N_{eff} is the effective number of

Table 2

Glacier-wide mean annual surface elevation changes ($\overline{\Delta h}$) and standard deviation ($\sigma_{\Delta h}$) of surface elevation changes over stable terrain and uncertainty of the geodetic mass balance (σ_{geod}).

Period	$\overline{\Delta h}$ (m a^{-1})	$\sigma_{\Delta h}$ (m a^{-1})	$\sigma_{geod.\ a}$ (m w.e. a^{-1})	B_{geod} (m w.e. a^{-1})
1981–2015	−0.63	± 0.16	± 0.14	−0.53 ± 0.14

independent measurements, calculated using the total number of measurements N_{tot},

$$N_{eff} = \frac{N_{tot} \cdot r}{2d} \tag{10}$$

and d is the distance of spatial autocorrelation (678 m), determined using Moran's autocorrelation index on the stable terrain elevation changes. Resulting values of $\sigma_{geod.\ a}$ are listed in Table 2.

The total random error of the geodetic method is different from that of the glaciological method due to the error propagation principle. The cumulative uncertainty of geodetic mass balance ($\sigma_{geod.\ PoR}$) over the PoR is expressed as:

$$\sigma_{geod.PoR} = \sigma_{geod.a} \cdot N \tag{11}$$

and was 4.76 m w.e. over the PoR.

5. Generic differences between glaciological and geodetic mass balances

A direct comparison of the glaciological and geodetic balances requires detailed analysis of the generic differences between the two methods. Note that Urumqi Glacier No.1 is a small and cold glacier (−8 to −1 °C for nearly the whole of the ice volume) with small ice velocity (Huang, 1999). Since the glacier has low driving stresses and reduced dynamics, hardly any crevasses and supraglacial meltwater channels, and hardly any frictional and strain heating and heat advection, internal and basal mass balances are insignificant compared to the uncertainty and cumulative glaciological mass balance. We mainly considered the following three sources.

5.1. Glacier density

One significant difference between the glaciological and geodetic mass balances is that the former is calculated using in situ measured densities; the geodetic surveys provide a glacier volume change, which needs to be converted into a change in mass using a density conversion. However, the density is difficult to determine and affects the accuracy of the geodetic mass balance (Zemp et al., 2013). In order to quantify the sensitive of the geodetic mass balance to the density conversion, here three density scenarios were implemented. Scenario (a): no changes in the vertical firn density profile occur over time in the accumulation area (Bader, 1954). Often an ice density (900 kg m^{-3}) is used as the conversion (e.g. Andreassen, 1999; Thibert et al., 2008). Scenario (b): use of zonally variable conversion, the density below the balanced-budget ELA (ELA$_0$) is 900 kg m^{-3} for glacier surface changes over ice and above the ELA$_0$ is 600 kg m^{-3} for surface changes over snow and firn (e.g. Kääb et al., 2012; Basantes-Serrano et al., 2016). ELA$_0$ is derived from the linear regression between ELA and specific glaciological annual mass balance (Zemp et al., 2010). Resulting value of ELA$_0$ was 3990 m a.s.l over the PoR. Scenario (c): we used a recommended density conversion of 850 ± 60 kg m^{-3} for the volume-to-mass conversion based on an empirical firn densification model with idealized surface mass balance forcing (Huss, 2013). The conversion is recommended in the case of a geodetic observation span longer than 5 years, with stable mass balance gradients, volume changes significantly different from zero and a firn area exists (Huss, 2013). Despite the equilibrium-line altitude (ELA) of Urumqi Glacier No.1 rising

during the PoR, a significant firn area was always present in each year except for 2010, when ELA surpassed the glacier summit. The statistical average accumulation-area ratio (AAR) was 40% (Fig. 5a and b). Therefore, the recommended density conversion by Huss (2013) is applicable. This conversion has been widely used in similar studies (e.g. Andreassen et al., 2016; Thomson et al., 2017; Galos et al., 2017).

The cumulative geodetic mass balances under the three scenarios (a), (b) and (c), were −19.20, −16.90 and −18.13 m w.e., respectively. The maximum difference (2.30 w.e.) between the three density scenarios was much less than the uncertainty of the geodetic mass balance. The geodetic mass balance under scenario (b) is very close to the average of the three scenarios (−18.08 w.e.), we therefore used a density conversion of 850 ± 60 kg m^{-3}.

5.2. Reference glacier area

The geodetic method uses the mean glacier area of the two geodetic times. The conventional glaciological method actually requires updated glacier outlines for every year (Elsberg et al., 2001; Huss et al., 2012). However, annual surveys of glacier boundary are impossible for most glaciers. The reference area used to calculate the glaciological mass balance of Urumqi Glacier No.1 may result in cumulative errors. Changes in glacier area and its impact on the calculation of glacier-wide mass balance of Urumqi Glacier had been studied by using nine topographic maps from 1962 to 2006 (annual areas were calculated by assuming a linear change in the glacier surface area), and the results indicated that reference-surface annual mass balances were slight less negative than the conventional ones (Wang and Shen, 2011). Since the glacier mapping had been implemented at the interval of 2–3 years since 2006 (Wang et al., 2016), we conservatively used the error term of Wang and Shen (2011). The cumulative differences between glacier-wide conventional and reference-surface mass balance were in the range of 0.32–0.73 m w.e. with an average value of 0.56 m w.e. over the PoR.

5.3. Different survey dates

Generally, it is difficult to guarantee the glaciological measurements and geodetic surveys are carried out at the same time. A comparison between the two methods needs to account for the surveying-day differences. Fortunately, the two DEMs were captured at the end of the ablation season and coincide closely with the days of the glaciological measurements. Mass balance processes of Urumqi Glacier No.1 mainly occur in summer and the glacier is dominated by weak accumulation in winter (Liu et al., 1997). The difference related to observation dates can therefore be considered negligible.

6. Results

6.1. Surface elevation and geodetic mass changes

The map of the geodetic elevation changes presents a strong ice loss at lower elevations and smaller thinning to slight thickening at higher elevations during the PoR, and the elevation changes mainly range from −1 to −0.1 m (Fig. 7). The mean elevation change was −0.63 ± 0.16 m a^{-1}, with a total change of −21.33 ± 5.44 m. The proportion of thinning area was about 88.3% of the entire glacier. Reduced glacier surface elevation occurred mainly in the ablation areas and on the right edge of the east branch. The latter has a steeper topography (Figs. 1 and 9c) and receives more shortwave-radiation (Bai et al., 1989; Yue et al., 2017), which may be adverse to mass accumulation. In addition, the steep slope also increases the removal of large snow depositions by avalanches. The elevation changes measured along the main flow line allow more detailed insights into the characteristics of the glacier behavior. The east and west branch show that the ice thinning continuously decreased with increasing altitude. In the
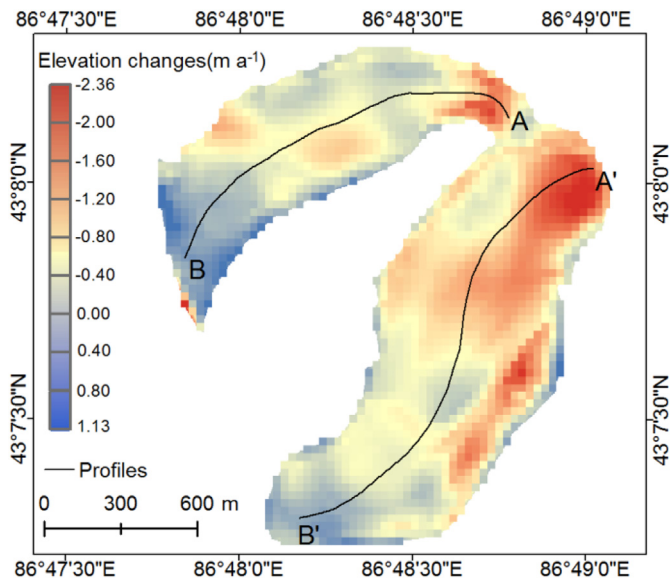
Fig. 7. Spatial distribution of annual surface elevation changes by differencing of the two DEMs between 1981 and 2015. Pronounced surface elevation lowering occurred across the ablation area with smaller thinning to slight thickening in the upper-elevation parts. Black lines indicate longitudinal profiles.

upper most parts of the glacier even a slight thickening was observed (Fig. 8). All of these results agree well with the long-term in situ measurements. Table 2 shows the glacier-wide mass balance and its uncertainty, the calculation of geodetic mass balance across the average glacier extent (1.71 km²) was −0.53 ± 0.14 m w.e. a⁻¹ or −18.13 ± 4.76 m w.e. during the PoR.

6.2. Comparison of glaciological and geodetic mass balances

In the long-term glaciological mass-balance time series of Urumqi Glacier No.1, an average correction of 0.56 m w.e. was used to convert the cumulative reference-surface mass balance (−16.12 m w.e.) to a conventional mass balance (−15.56 m w.e.). Since the uncertainty duo to changes in acquisition dates of the two DEMs used can be ignored, the resulting glaciological and geodetic mass balances are comparable. The reduced discrepancy δ between the cumulative glaciological and the geodetic mass balances can be calculated as

$$\delta = \frac{\Delta_{\text{PoR}}}{\sigma_{\text{common.PoR}}} = \frac{B_{\text{glac.PoR}} - B_{\text{geod.PoR}}}{\sqrt{\sigma_{\text{glac.PoR}}^2 + \sigma_{\text{geod.PoR}}^2}} \tag{12}$$

where Δ_{PoR} is the difference between the cumulative glaciological and geodetic mass balances (2.57 m w.e.). Here $\sigma_{\text{common. PoR}}$ is the common variance of the two methods (4.83 m w.e.), which is defined as the combined random uncertainties of the two methods, according to the principle of error propagation (Zemp et al., 2013). As the reduced discrepancy (δ = 0.53) falls within the 95% confidence interval ($|\delta| < 1.96$), agreement between the glaciological and geodetic methods can be considered as satisfying.

Although the observed difference (0.08 m w.e. a⁻¹) between the two methods is not statistically significant, being less than the random error (0.14 m w.e. a⁻¹) of the glaciological method, it is necessary to conduct sensitivity of the parameter. Holding the density conversion (850 ± 60 kg m⁻³) fixed and we find that allowing the correction between conventional and reference-surface mass balance to range from 0.32 to 0.73 m w.e. leads to a maximum difference of 2.74 m w.e. when the correction is 0.73 m w.e., the reduced discrepancy (δ = 0.57) also falls within the 95% confidence interval ($|\delta| < 1.96$). When holding the correction (0.56 m w.e.) fixed, the density scenarios (a) and (b) (see Section 5.1) result in the difference of 3.64 and 1.34 m w.e., respectively, the former of which calculates a value of δ = 0.75 and the discrepancy continues to fall within the 95% confidence interval. If we combine the maximum corrected value (0.73 m w.e.) with density
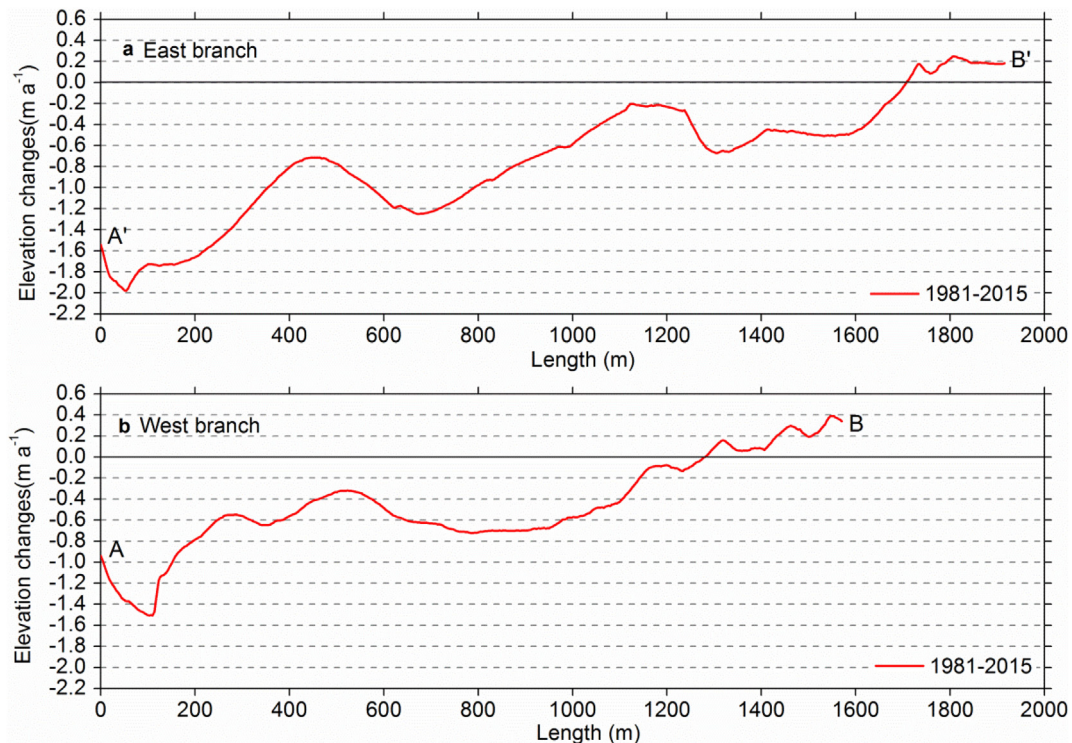

Fig. 8. Longitudinal profiles of annual surface elevation changes of east (a) and west branch (b) over the PoR. The capital letters presented here are really same as Fig. 7.

Fig. 9. Photographs of Urumqi Glacier No.1 surface characteristic taken at the end of ablation season. (a) steep slope in tongue of the west branch are prone to ice avalanches. (b) Supraglacial river. (c) Precipitous terrain on the upper right edge of the east branch.

scenario (a), resulting discrepancy ($\delta = 0.79$) still remains within the 95% confidence interval. A calibration of the glaciological record is therefore currently not necessary.

7. Discussion

7.1. Difference analysis

The geodetic mass balance remains more negative compared to cumulative glaciological ones; it is possible that the more negative mass balance is relevant to glacier surface characteristics, including:

(1) With the accelerated retreat of Urumqi Glacier No.1, the glacier snout of the west branch has become increasingly steep, and is prone to ice avalanches in the ablation season (Fig. 9a), according to field observations.
(2) An extensive supraglacial river exists due to strong ablation (Fig. 9b). This process may have increased the energy of shortwave-radiation to transport into the glacier, including the potential energy released by flowing water, and it also increases the effective ablation area.
(3) The precipitous terrain on the upper right edge of the east branch (Figs. 1 and 9c) has obviously thinned (Fig. 7a).

The mass loss from the first two items cannot be well quantified by the glaciological measurements. The third makes it difficult to insert stakes and dig snow pits in this steep terrain. Unrepresentative distribution of stakes has significant influence on extrapolating point observations to glacier-wide mass balance (Cox and March 2004). The steep terrain increases the removal of large snow depositions by avalanches, resulting in surface albedo of the upper right edge was in the range of 0.2–0.4 at the end of the ablation season and clearly lower than the left elevation bands (Yue et al., 2017). Therefore, mass balance may be overestimated when we calculate glacier-wide mass balance using the glaciological method.

In addition, the spatial resolution of the topographic map is relative low compared to TLS-derived DEM, the coarse DEM tends to overestimate the altitude in deep troughs, like the supraglacial river, where the curvature of the terrain is highly negative (Ruiz et al., 2017). This would probably result in underestimating the geodetic mass balance. Excluding the resolution of DEMs, density conversion is still a major error in the calculation of geodetic mass balance, which can become the potential source of the discrepancy between the two methods.

7.2. Comparison to previous similar studies

In order to assess the quality of the geodetic and glaciological mass balances and investigate whether the difference between the two methods also occurs in other regions and climate setting, our results is compared to previous similar studies. On Griesgletscher (Switzerland), Huss et al. (2009) computed the annual uncertainty of ± 0.14 m w.e. a^{-1} for the geodetic mass changes. Barandun et al. (2015) quantified the value of $\sigma_{geod.\ a} = \pm 0.17$ m w.e. a^{-1} for Abramov glacier (Kyrgyzstan). The accuracy of our results measured with geodetic method is thus similar to the above mentioned uncertainties. Since this paper only obtains one high-resolution DEM from the TLS surveys, the uncertainty in the geodetic mass balance derived from multi-temporal high-quality DEMs is obviously smaller than our results (e.g. Joerg et al., 2012; Galos et al., 2017; Klug et al., 2018). Annul uncertainty in the glacier-wide glaciological mass balance presented here is close to those studies for Sarennes, French (Thibert et al., 2008) and Glaciar Antisana 15α, Ecuador (Basantes-Serrano et al., 2016) (the annual error in the specific glaciological mass balance was 0.16 m w.e. a^{-1} for both glaciers), but smaller than other measured glaciers (e.g. Thomson et al., 2017; Klug et al., 2018). This is probably due to higher density of annual point measurements (Figs. 4 and 5c) and smaller surface area of Urumqi Glacier No.1 than aforementioned glaciers (WGMS, 2017). Therefore, the quality of the glaciological and geodetic mass balances is relative good.

Table 3 compares the mean annul difference (Δ_{PoR}/N) between Urumqi Glacier No.1 and others in different regions. The difference ranged from −0.20 to 0.39 m w.e. a^{-1}, and the corresponding value of

Table 3
Cumulative specific geodetic (B_{geod}) and glaciological (B_{glac}) mass balance of selected glaciers in different regions (in m w.e.). The difference between the two methods is divided by the time spans (N) to calculate the mean annul difference.

Glacier	Period	B_{geod}	B_{glac}	Δ_{PoR}/N	Source
Tuyuksu (KZ)	1958–1998	−12.60	−16.80	0.11	Hagg et al. (2004)
Gulkana (US)	1974–1999	−11.80	−11.20	−0.02	Cox and March (2004)
Sarennes (FR)	1952–2003	−32.30	−34.89	0.05	Thibert et al. (2008)
Storglaciären (SE)	1959–1999	−4.89	−3.93	−0.02	Zemp et al. (2010)
Hintereisferner (AT)	1953–2006	−35.00	−27.70	−0.10	Fischer (2011)
Bahía del Diablo (AQ)	2001–2011	−2.16	−1.90	−0.03	Marinsek and Ermolin (2015)
Glaciar Antisana 15α (EC)	1997–2009	−1.39	−6.05	0.39	Basantes-Serrano et al. (2016)
White (CA)	1960–2014	−9.61	−11.50	−0.04	Thomson et al. (2017)
Hintereisferner (AT)	2001–2011	−13.41	−12.19	0.12	Klug et al. (2018)
Urumqi Glacier No.1 (CN)	1981–2015	−18.13	−16.12	0.08	This study

Note: KZ - Kazakhstan, US - United States of America, FR - France, SE – Sweden, AT – Austria, AQ – Antarctica, EC – Ecuador, CA – Canada, and CN – China.

Urumqi Glacier No.1 is within this range and very close to Sarennes, but significant smaller than Glaciar Antisana 15α. This can be explained by underestimated net accumulation in the upper elevations of Glaciar Antisana 15α, resulting in a too negative specific glaciological mass balance (Basantes-Serrano et al., 2016).

7.3. Recommendations for future monitoring

Advantages and shortcomings are inherent in both methods to monitor glacier mass balance; a combination of the glaciological measurements and TLS surveys may yield optimum results. We recommend the use of Riegl VZ®-6000 TLS to monitor the mass balance of Urumqi Glacier No.1. The long-range capability of the TLS is perfectly suited to monitor the inaccessible glacier areas (e.g. crevasses, steep terrain and debris cover, etc.) and quantify the mass loss due to ice avalanches, and what's more, the TLS device allows a monitoring having a high temporal-spatial resolution. Now the application and validation of long-range TLS for monitoring the annual geodetic mass balance has already been done (e.g. Fischer et al., 2016). To gain added value about the applicability of repeated TLS surveys to monitor glacier mass balance and detect possible difference between the two methods on a monthly basis, we may consider performing monthly TLS surveys since glaciological monthly net mass balances of Urumqi Glacier No.1 are measured in summer. High-quality TLS-derived monthly net mass balance cloud be obtained depended mainly on (1) plentiful and visible areas of stable bedrock terrain surrounding the whole glacier, leading to better precision of the relative registration of consecutive TLS point clouds; (2) a good weather condition (dry and windless atmosphere); and (3) a reliable density conversion of volume changes to mass balance. Nevertheless, a density conversion becomes more challenging over short time periods because of meteorological influences on the elevation changes (Huss, 2013). Urumqi Glacier No.1 is a summer-accumulation-type glacier; strong ablation and accumulation occur simultaneously in summer (Liu et al., 1997). Glacier thickness changes in ice, snow and firn usually occur at the same vertical profile at the strong ablation season according to in situ measurements. We had presented the use of long-rang TLS to monitor the monthly net mass balance of Urumqi Glacier No.1 at the beginning of the ablation season (May–June), the abundance of fresh snow affected the accuracy of the TLS-derived geodetic mass balance (Xu et al., 2017). Therefore, the time when the small amount of fresh snow covers the glacier should be selected to carry out both the TLS surveys and glaciological measurements. TLS-derived geodetic monthly net mass balance could be calculated from the multiplication of monthly glacier volume changes with in situ measured densities of firn and snow. Then detailed comparisons between TLS-derived and glaciological mass balance can be implemented at the monthly scale.

Moreover, it is also important to note that the velocity of Urumqi Glacier No.1 has been decreasing and the annual average velocity was reduced by 1.3% from 1980/1981 to 2011/2012 (Wang et al., 2017). The reduced velocity can increase glacier thickness in the accumulation area, but the lack of observed velocity data in the upper elevations prevents a more detailed quantitative analysis. Further studies, using physics-based models to understand better the glacier dynamics are recommended.

8. Conclusions

It has become an international monitoring standard to periodically reanalyze, and if necessary, calibrate the glaciological mass balance series with high-quality products of geodetic surveys over the past several decades. Here we have compared accurate geodetic results with long-term glaciological mass balance records from 1981 to 2015 for Urumqi Glacier No.1, including in-depth uncertainties assessments. The geodetic mass balance (-18.13 m w.e.) and corrected cumulative glaciological mass balance (-15.56 m w.e.) confirm that Urumqi Glacier

No.1 had experienced a continuous mass loss over the PoR. Our results show that the good agreement between two methods on Urumqi Glacier No.1 is promising and confirms the excellent quality of the glaciological mass balance data and a calibration is hence currently not required. The more negative geodetic mass balance is probably relevant to the glacier surface characteristics.

The uncertain analysis revealed that the main errors of the glaciological method can be attributed to field measurements and the extrapolation of point values to glacier-wide mass balance. The annul uncertainty in the specific glaciological mass balance (± 0.14 m w.e. a^{-1}) was smaller than some measured glaciers worldwide, probably due to the dense point measurements and relative small area of Urumqi Glacier No.1. Uncertainties in the geodetic mass balance are mainly related to the accuracy of the topographic map used and the corresponding annual uncertainty was close to many similar studies, but bigger than those derived from multi-temporal high-quality DEMs.

It is important to continue the long-term mass-balance series, especially for regions like Central Asia; such information is of fundamental importance for water resource management. The geodetic results derived by the long-range TLS surveys can calibrate the glaciological mass balances. In further studies, the TLS system should be used to attempt better quantification of the influence of ice avalanches and glacier surface terrain. Detailed comparisons between the glaciological and geodetic monthly net mass balances at the ablation season are necessary.

References

Andreassen, L.M., 1999. Comparing traditional mass balance measurements with long-term volume change extracted from topographical maps: a case study of Storbreen glacier in Jotunheimen, Norway, for the period 1940–1997. Geogr. Ann. 81A (4), 467–476.

Andreassen, L.M., Elvehøy, H., Kjøllmoen, B., Engeset, R.V., 2016. Reanalysis of long-term series of glaciological and geodetic mass balance for 10 Norwegian glaciers. Cryosphere 10, 535–552. https://doi.org/10.5194/tc-10-535-2016.

Bader, H., 1954. Sorge's law of densification of snow on high polar glaciers. J. Glaciol. 2, 319–323.

Bai, Z., Tetsuo, O., Keiji, H., 1989. Calculation results of radiational climate in glacierized cirque and glacier-free cirque at the headwater of Urumqi River in Tianshan Mountains. J. Glaciol. Geocryol. 11 (4), 336–349.

Barandun, M., Huss, M., Sold, L., Farinotti, D., Azisov, E., Salzmann, N., Usulbaliev, R., Merkushkin, A., Hoelzle, M., 2015. Re-analysis of seasonal mass balance at Abramov glacier 1968-2014. J. Glaciol. 61 (230), 1103–1117. https://doi.org/10.3189/2015JoG14J239.

Basantes-Serrano, R., Rabatel, A., Francou, B., Vincent, C., Maisincho, L., Cáceres, B., Galarraga, R., Alvarez, D., 2016. Slight mass loss revealed by reanalyzing glacier mass balance observations on Glaciar Antisana 15 during the 1995–2012 period. J. Glaciol. 62 (231), 124–136. https://doi.org/10.1017/jog.2016.17.

Besl, P., McKay, N., 1992. A method for registration of 3-D shapes. IEEE Trans. Pattern Anal. Mach. Intell. 14 (2), 239–256.

Bolch, T., Pieczonka, T., Mukherjee, K., Shea, J., 2017. Brief communication: Glaciers in the Hunza catchment (Karakoram) have been nearly in balance since the 1970s. Cryosphere 11 (531), 531–539. https://doi.org/10.5194/tc-11-531-2017.

Chen, J.M., Liu, C.H., Jin, M., 1996. Application of the repeated aerial photogrammetry to monitoring glacier variation in the drainage area of the Urumqi River. J. Glaciol. Geocryol. 18 (4), 331–3364.

Cogley, J.G., 2009. Geodetic and direct mass-balance measurements: comparison and joint analysis. Ann. Glaciol. 50 (50), 96–100. https://doi.org/10.3189/172756409787769744.

Cogley, J.G., Hock, R., Rasmussen, L.A., Arendt, A.A., Bauder, A., Braithwaite, R.J., Jansson, P., Kaser, G., Möller, M., Nichol-Son, L., Zemp, M., 2011. Glossary of Glacier Mass Balance and Related Terms. (IHP-VII Technical Documents in Hydrology No. 86, IACS Contribution No. 2). UNESCO–International Hydrological Programme, Paris.

Cox, L.H., March, R.S., 2004. Comparison of geodetic and glaciological mass-balance

techniques, Gulkana Glacier, Alaska, U.S.A. J. Glaciol. 50 (170), 363–370. https://doi.org/10.3189/172756504781829855.

Deems, J.S., Painter, T.H., Finnegan, D.C., 2013. Lidar measurement of snow depth: a review. J. Glaciol. 59 (215), 467–479. https://doi.org/10.3189/2013JoG12J154.

Dyurgerov, M.B., 2002. Glacier mass balance and regime: data of measurements and analysis. In: Meier, M.F., Armstrong, R. (Eds.), Occasional Paper. Institute of Arctic and Alpine Research Vol. 55. University of Colorado, Boulder, Colorado, pp. 21–40.

Elsberg, D.H., Harrison, W.D., Echelmeyer, K.A., Krimmel, R.M., 2001. Quantifying the effects of climate and surface change on glacier mass balance. J. Glaciol. 47 (159), 649–658.

Farinotti, D., Longuevergne, L., Moholdt, G., Dustman, D., Mölg, T., Bolch, T., 2015. Substantial glacier mass loss in the Tien Shan over the past 50 years. Nat. Geosci. 8, 716–722. https://doi.org/10.1038/ngeo2513.

Fischer, A., 2011. Comparison of direct and geodetic mass balances on a multi-annual time scale. Cryosphere 5, 107–124. https://doi.org/10.5194/tc-5-107-2011.

Fischer, M., Huss, M., Kummert, M., Hoelzle, M., 2016. Application and validation of long-range terrestrial laser scanning to monitor the mass balance of very small glaciers in the Swiss Alps. Cryosphere 10, 1279–1295. https://doi.org/10.5194/tc-10-1279-2016.

Gabbud, C., Micheletti, N., Lane, S.N., 2015. Lidar measurement of surface melt for a temperate Alpine glacier at the seasonal and hourly scales. J. Glaciol. 61 (299), 963–974. https://doi.org/10.3189/2015JoG14J226.

Galos, S.P., Klug, C., Maussion, F., Covi, F., Nicholson, L., Rieg, L., Gurgiser, W., Mölg, T., Kaser, G., 2017. Reanalysis of a 10-year record (2004–2013) of seasonal mass balances at Langenferner/Vedretta Lunga, Ortler Alps, Italy. Cryosphere 11, 1417–1439. https://doi.org/10.5194/tc-11-1417-2017.

Gardelle, J., Berthier, E., Arnaud, Y., Kääb, A., 2013. Region-wide glacier mass balances over the Pamir–Karakoram–Himalaya during 1999–2011. Cryosphere 7, 1263–1286. https://doi.org/10.5194/tc-7-1263-2013.

GB/T 12343.1-2008, 2008. Compilation Specifications for National Fundamental Scale Maps—Part 1: Compilation Specifications for 1: 25 000/1: 50 000/1: 100 000 Topographic Maps. General Administration of Quality Supervision, Inspection and Quarantine of the People's Republic of China and Standardization Administration of the People's Republic of China, Beijing, pp. 1–40.

Hagg, W.J., Braun, L.N., Uvarov, V.N., Makarevich, K.G., 2004. A comparison of three methods of mass-balance determination in the Tuyuksu glacier region, Tien Shan, Central Asia. J. Glaciol. 50 (171), 505–510. https://doi.org/10.3189/172756504781829783.

Han, T., Liu, S., Ding, Y., Jiao, K., 2005. A characteristics mass balance of glacier No. 1 at the headwaters of the Urumqi River, Tianshan Mountains. Adv. Earth Sci. 20 (3), 298–303.

Hartzell, P.J., Gadomski, P.J., Glennie, C.L., Finnegan, D.C., Deems, J.S., 2015. Rigorous error propagation for terrestrial laser scanning with application to snow volume uncertainty. J. Glaciol. 61 (230), 1147–1158. https://doi.org/10.3189/2015JoG15J031.

Helfricht, K., Kuhn, M., Keuschnig, M., Heilig, A., 2014. Lidar snow cover studies on glaciers in the Ötztal Alps (Austria): comparison with snow depths calculated from GPR measurements. Cryosphere 8, 41–57. https://doi.org/10.5194/tc-8-41-2014.

Hock, R., Jensen, H., 1999. Application of kriging interpolation for glacier mass balance computations. Geogr. Ann. A. 81 (4), 611–619. https://doi.org/10.1111/1468-0459.00089.

Huang, M.H., 1999. Forty year's study of glacier temperature in China. J. Glaciol. Geocryol. 21 (3), 193–199.

Huss, M., 2013. Density assumptions for converting geodetic glacier volume change to mass change. Cryosphere 7 (3), 877–887. https://doi.org/10.5194/tc-7-877-2013.

Huss, M., Bauder, A., Funk, M., 2009. Homogenization of long-term mass-balance time series. Ann. Glaciol. 50 (50), 198–206. https://doi.org/10.3189/172756409787769627.

Huss, M., Hock, R., Bauder, A., Funk, M., 2012. Conventional versus reference-surface mass balance. J. Glaciol. 58, 278–286. https://doi.org/10.3189/2012JoG11J216.

Jansson, P., Pettersson, P., 2007. Spatial and temporal characteristics of a long mass balance record, Storglaciären, Sweden. Arct. Antarct. Alp. Res. 39 (3), 432–437.

Joerg, P., Morsdorf, F., Zemp, M., 2012. Uncertainty assessment of multi-temporal airborne laser scanning data: a case study at an Alpine glacier. Remote Sens. Environ. 127, 118–129. https://doi.org/10.1016/j.rse.2012.08.012.

Kääb, A., Berthier, E., Nuth, C., Gardelle, J., Arnaud, Y., 2012. Contrasting patterns of early 21st century glacier mass change in the Himalaya. Nature 488, 495–498. https://doi.org/10.1038/nature11324.

Kaser, G., Fountain, A.G., Jansson, P., 2003. A Manual for Monitoring the Mass Balance of Mountain Glaciers. (IHP-VI Technical Documents in Hydrology 59). UNESCO, Paris, pp. 9–54.

Kaser, G., Cogley, J.G., Dyurgerov, M.B., Meier, M.F., Ohmura, A., 2006. Mass balance of glaciers and ice caps: consensus estimates for 1961–2004. Geophys. Res. Lett. 33 (19), L19501. https://doi.org/10.1029/2006GL027511.

Klug, C., Bollmann, E., Galos, S.P., Nicholson, L., Prinz, R., Rieg, L., Sailer, R., Stötter, J., Kaser, G., 2018. Geodetic reanalysis of annual glaciological mass balances (2001−2011) of Hintereisferner, Austria. Cryosphere 12, 833–849. https://doi.org/10.5194/tc-12-833-2018.

Li, Z.Q., 2005. A glacier melt water pool was discovered at summit of east branch of Glacier No. 1 at Urumqi River Head, Tianshan Mts., Xinjiang. J. Glaciol. Geocryol. 27 (1), 150–152 (in Chinese).

Li, Z.Q., Wang, W.B., Zhang, M.J., Wang, F.T., Li, H.L., 2010. Observed changes in stream flow at the headwater of the Urumqi River, eastern Tianshan, central Asia. Hydrol. Process. 24 (2), 217–224. https://doi.org/10.1002/hyp.7431.

Li, Z.Q., Li, H.L., Chen, Y.N., 2011. Mechanisms and simulation of accelerated shrinkage of continental glaciers: a case study of Urumqi Glacier No. 1 in Eastern Tianshan,

central Asia. J. Earth Sci. 22 (4), 423–430. https://doi.org/10.1007/s12583-011-0194-5.

Lichti, D.D., Gordon, S.J., Tipdecho, T., 2005. Error models and propagation in directly georeferenced terrestrial laser scanner networks. J. Surv. Eng. 131 (4), 135–142. https://doi.org/10.1061/(ASCE)0733-9453(2005)131:4(135).

Liu, C., Xie, Z.C., Wang, C.Z., 1997. A research on the mass balance process of Glacier No.1 at the headwaters of the Urumqi River, Tianshan Mountains. J. Glaciol. Geocryol. 19 (1), 17–24 (in Chinese).

Marinsek, S., Ermolin, E., 2015. 10 year mass balance by glaciological and geodetic methods of Glaciar Bahía del Diablo, Vega Island, Antarctic Peninsula. Ann. Glaciol. 56 (79), 141–146. https://doi.org/10.3189/2015AoG70A958.

Meier, M.F., Tangborn, W.V., Mayo, L.R., Post, A., 1971. Combined ice and water balances of Gulkana and Wolverine Glaciers, Alaska, and South Cascade Glacier, Washington, 1965 and 1966 hydrologic years. USGS Prof. Pap. 715-A.

Mukupa, W., Roberts, G.W., Hancock, C.M., Almanasir, K., 2016. A review of the use of terrestrial laser scanning application for change detection and deformation monitoring of structures. Surv. Rev. 1-18. https://doi.org/10.1080/00396265.2015.1133039.

Nuth, C., Kääb, A., 2011. Co-registration and bias corrections of satellite elevation data sets for quantifying glacier thickness change. Cryosphere 5 (1), 271–290. https://doi.org/10.5194/tc-5-271-2011.

Østrem, G., Brugman, M., 1991. Glacier Mass Balance Measurements: A Manual for Field and Office Work. Environment Canada, National Hydrology Research Institute, Saskatoon, SK (NHRI Science Report 4.).

Paul, F., Haeberli, W., 2008. Spatial variability of glacier elevation changes in the Swiss Alps obtained from two digital elevation models. Geophys. Res. Lett. 35 (21), L21502. https://doi.org/10.1029/2008GL034718.

Perroy, R.L., Bookhagen, B., Asner, G.P., Chadwick, O.A., 2010. Comparison of gully erosion estimates using airborne and ground-based LiDAR on Santa Cruz Island, California. Geomorphology 118 (3), 288–300. https://doi.org/10.1016/j.geomorph.2010.01.009.

Piermattei, L., Carturan, L., Guarnieri, A., 2015. Use of terrestrial photogrammetry based on structure-from-motion for mass balance estimation of a small glacier in the Italian Alps. Earth Surf. Process. Land. 40 (13), 1791–1802. https://doi.org/10.1002/esp.3756.

Rabatel, A., Deline, P., Jaillet, S., Ravanel, L., 2008. Rock falls in high-alpine rock walls quantified by terrestrial LiDAR measurements: a case study in the Mont Blanc area. Geophys. Res. Lett. 35 (10), L10502. https://doi.org/10.1029/2008GL033424.

RIEGL Laser Measurement Systems, 2013. Preliminary Data Sheet, 07.05.2013; Riegl VZ-6000 – 3D Ultra Long Range Terrestrial Laser Scanner with Online Waveform Processing. RIEGL Laser Measurement Systems, Horn, Austria.

RIEGL Laser Measurement Systems, 2014a. 3D Terrestrial Laser Scanner Riegl VZ®-4000/ Riegl VZ®-6000 General Description and Data Interfaces. RIEGL Laser Measurement Systems, Horn, Austria.

RIEGL Laser Measurement Systems, 2014b. RiSCAN PRO® – Version 1.8.1. Riegl Laser Measurement Systems, Horn, Austria.

Ruiz, L., Berthier, E., Viale, M., Pitte, P., Masiokas, M.H., 2017. Recent geodetic mass balance of Monte tronador glaciers, northern Patagonian Andes. Cryosphere 11, 619–634. https://doi.org/10.5194/tc-11-619-2017.

Schnabel, R., Klein, R., 2006. Octree-based point-cloud compression. In: Proceedings of Eurographics Symposium on Point Based Graphics, Boston, MA, USA, pp. 111–120. https://doi.org/10.2312/SPBG/SPBG06/111-120.

Shangguan, D.H., Liu, S.Y., Ding, Y.J., Zhang, Y., Li, J., Li, X.Y., Wu, Z., 2010. Changes in the elevation and extent of two glaciers along the Yanglonghe River, Qilian Shan, China. J. Glaciol. 56 (196), 309–317. https://doi.org/10.3189/002214310791968566.

Thibert, E., Vincent, C., 2009. Best possible estimation of mass balance combining glaciological and geodetic methods. Ann. Glaciol. 50, 112–118. https://doi.org/10.3189/172756409787769546.

Thibert, E., Blanc, R., Vincent, C., Eckert, N., 2008. Glaciological and volumetric mass-balance measurements: error analysis over 51 years for Glacier de Sarennes, French Alps. J. Glaciol. 54 (186), 522–532. https://doi.org/10.3189/002214308785837093.

Thomson, L.I., Zemp, M., Copland, L., Cogley, J.G., Ecclestone, M.A., 2017. Comparison of geodetic and glaciological mass budgets for White Glacier, Axel Heiberg Island, Canada. J. Glaciol. 63 (237), 55–66. https://doi.org/10.1017/jog.2016.112.

Wang, G.Y., Shen, Y.P., 2011. The effect of change in glacierized area on the calculation of mass balance in the Glacier No.1 at the headwaters of Urumqi River. J. Glaciol. Geocryol. 33 (1), 1–7 (in Chinese).

Wang, S.J., Zhang, M.J., Li, Z.Q., Wang, F.T., Li, H.L., Li, Y.J., Huang, X.Y., 2011. Response of glacier area variation to climate change in Chinese Tianshan mountains in the past 50 years. Acta Geograph. Sin. 66 (1), 38–46 (in Chinese).

Wang, P.Y., Li, Z.Q., Li, H.L., Yao, H.B., Xu, C.H., Zhou, P., Jin, S., Wang, W.B., 2016. Analyses of recent observations of Urumqi Glacier No. 1, Chinese Tianshan Mountains. Environ. Earth Sci. 75 (8), 1–11. https://doi.org/10.1007/s12665-016-5551-3.

Wang, P.Y., Li, Z.Q., Zhou, P., Li, H.L., Yu, G.B., Xu, C.H., Wang, L., 2017. Long-term change in ice velocity of Urumqi Glacier No. 1, Tian Shan, China. Cold Reg. Sci. Technol. 145, 177–184. https://doi.org/10.1016/j.coldregions.2017.10.008.

Wei, J.F., Liu, S.Y., Guo, W., Xu, J.L., Bao, W.J., Shangguan, D.H., 2015. Changes in glacier volume in the north bank of the Bangong Co basin from 1968 to 2007 based on historical topographic maps, SRTM, and ASTER stereo images. Arct. Antarct. Alp. Res. 47 (2), 301–311. https://doi.org/10.1657/AAAR00C-13-129.

World Glacier Monitoring Service (WGMS), 2017. Global Glacier Change Bulletin No. 2 (2014–2015). In: Zemp, M., Nussbaumer, S.U., Gärtner-Roer, I., Huber, J., Machguth, H., Paul, F., Hoelzle, M. (Eds.), ICSU(WDS)/IUGG(IACS)/UNEP/UNESCO/WMO. World Glacier Monitoring Service, Zurich, pp. 1–7. https://doi.org/10.5904/wgms-

fog-2017-10.

Xie, Z.C., Liu, C.H., 1991. Measurement method and main characteristics of the glacier mass balance in Asia. In: Application of Geographic Information Systems in Hydrology and Water Resources (ed. by K. Kovar & H. P. Nachtnabel) (Proc. HydroGIS 93 Conference, Vienna, April 1993), 453–459. IAHS Publ. no. 211.

Xie, Z.C., Liu, C.H., 2010. Introduction to Glaciology. Shanghai Popular Science Press, Shanghai, pp. 1–490 (in Chinese).

Xu, C.H., Li, Z.Q., Wang, F.T., Li, H.L., Wang, W.B., Wang, L., 2017. Using an ultra-long-range terrestrial laser scanner to monitor the net mass balance of Urumqi Glacier No. 1, eastern Tien Shan, China, at the monthly scale. J. Glaciol. 63 (241), 792–802. https://doi.org/10.1017/jog.2017.45.

Yue, X.Y., Zhao, J., Li, Z.Q., Zhang, M.J., Fan, J., Wang, L., Wang, P.Y., 2017. Spatial and temporal variations of the surface albedo and other factors influencing Urumqi Glacier No. 1 in Tien Shan, China. J. Glaciol. 63 (241), 899–911. https://doi.org/10.1017/jog.2017.57.

Zemp, M., Hoelzle, M., Haeberli, W., 2009. Six decades of glacier mass-balance observations: a review of the worldwide monitoring network. Ann. Glaciol. 50 (50), 101–111. https://doi.org/10.3189/172756409787769591.

Zemp, M., Jansson, P., Holmlund, P., Gärtner-Roer, I., Koblet, T., Thee, P., Haeberli, W., 2010. Reanalysis of multi-temporal aerial images of Storglaciären, Sweden (1959–99). Part 2: comparison of glaciological and volumetric mass balances. Cryosphere 4, 345–357. https://doi.org/10.5194/tc-4-345-2010.

Zemp, M., Thibert, E., Huss, M., Stumm, D., Rolstad Denby, C., Nuth, C., Nussbaumer, S.U., Moholdt, G., Mercer, A., Mayer, C., Joerg, P.C., Jansson, P., Hynek, B., Fischer, A., Escher-Vetter, H., Elvehøy, H., Andreassen, L.M., 2013. Reanalysing glacier mass balance measurement series. Cryosphere 7, 1227–1245. https://doi.org/10.5194/tc-7-1227-2013.

Zemp, M., et al., 2015. Historically unprecedented global glacier decline in the early 21st century. J. Glaciol. 61 (228), 745–762. https://doi.org/10.3189/2015JoG15J017.

Zhang, Z.Y., 1992. Iterative point matching for registration of free-form curves. Int. J. Comput. Vis. 13, 119–152. https://doi.org/10.1007/BF01427149.